2015 Geosynthetics CONFERENCE Feb. 15-18 | Portland OR

Geosynthetics 2015
February 15-18, Portland, Oregon

Investigation of Post-Shear Surface Texture Characteristics of Geomembranes

D.C. Manheim, Global Waste Research Institute, Cal Poly, USA, dmanheim@calpoly.edu
N. Yesiller, Ph.D., Global Waste Research Institute, Cal Poly, USA, nyesille@calpoly.edu
J.L. Hanson, Ph.D., PE, Civil and Environmental Engineering Department, Cal Poly, USA, jahanson@calpoly.edu
J.P. Gourc, Ph.D., LTHE, Transfers, Hydrology, Environment, Polytech Grenoble, Université Joseph Fourier, France, Jean-Pierre.Gourc@ujf-grenoble.fr
L. Carbone, Ph.D., Department of Civil, Energy, Environment, and Materials Engineering, DICEAM, Mediterranea University of Reggio Calabria, Italy, laura.carbone@unirc.it
N. Moraci, Ph.D., Department of Civil, Energy, Environmental, and Materials Engineering, Mediterranea University of Reggio Calabria, Italy, nicola.moraci@unirc.it
P. Carrubba, Ph.D., Department of Civil, Architectural and Environmental Engineering, University of Padova, Italy, paolo.carrubba@unipd.it
P. Pavanello, Department of Civil, Architectural and Environmental Engineering, University of Padova, Italy, paolo.pavanello@unipd.it

ABSTRACT

2D and 3D surface characteristics of virgin and post-shear geomembranes were investigated using optical interferometry. Shear response of geonet-smooth geomembrane (INT1) and geocomposite-textured geomembrane (INT2) interfaces were determined using inclined plane tests at low normal stress representing landfill covers. Geomembrane surfaces were modified significantly due to shearing. For INT1, the static interface friction angle increased with shear deformation. Geonet ribs ploughed into the geomembrane creating permanent, spatially oriented indentations. Roughness, developed surface area, peak material volume, valley void volume, and natural volume increased, whereas absolute surface area remained similar. For INT2, the static interface friction angle decreased with shear displacement. The geomembrane asperities were deformed by the geotextile filaments from the geocomposite. The peak feature widths decreased and peak heights, valley depths, negative volume, and absolute surface area increased. Modified roughness of the smooth geomembrane and deformation mechanisms of the textured geomembrane correlated to the increased and decreased shear resistance, respectively.

1. INTRODUCTION

The use of multi-layered liner systems in containment facilities represents the state-of-the practice in the U.S. and Europe as well as other parts of the world (e.g., Qian et al. 2002, NRC 2007, Briançon et al. 2011, Moraci et al. 2014). Such liner systems consist of a combination of natural soil and geosynthetic layers. Soil-geosynthetic and geosynthetic-geosynthetic interfaces are common in multi-layered liner systems used for both bottom and cover liners. Common types of geosynthetics including geotextiles (GTs); geomembranes (GMs); geosynthetic clay liners (GCLs); geonets (GNs) and geotextile/geonet composites (GCs); and geogrids (GRs) have been used in containment facilities to differing extents.

Mechanical performance of liner systems on slopes is significant to ensure overall stability of containment systems. Several studies have been conducted to investigate geosynthetic to geosynthetic interface shear response over the last few decades (e.g., Jones and Dixon 1998, Triplett and Fox 2001, Ivy 2003, Li and Gilbert 2006, Palmeira 2009, Pitanga et al. 2011, Carbone et al. 2013a). Significant interactions that affected the condition of tested geosynthetics were reported. Modification of the roughness of textured geomembranes against GCLs and GTs was visually observed in interface shear tests (Triplett and Fox 2001, Hebeler et al. 2005, McCartney et al. 2005, Li and Gilbert 2006, Kim and Frost 2011). Wearing/abrasion of texture material as well as deformation of texture features were observed. For textured geomembrane-geotextile (GMT-GT) interfaces, Li and Gilbert (2006) indicated that post-peak strength reduction observed in the tests likely resulted from wearing of the geomembrane textures at a microscopic scale in repeated shear passes. Shear strength reduction was more pronounced at high normal stress levels (345 to 690 kPa) as compared to low normal stresses, when the same geomembrane specimen was repeatedly sheared against a virgin GT specimen, indicating that the microtexture polishing effect was enhanced at high normal stresses. Hebeler et al. (2005) described a micro- to macro-scale hook and loop shear mechanism for GMT and needle punched nonwoven (NPNW) GT interfaces. The level of interactions was influenced by stress level. At low stresses (<50 kPa), the shear strength was mobilized by surficial interactions between the geomembrane micro-texture and the outermost fibers of the NPNW geotextile. At high stress levels (50-300 kPa) a matrix compression of the geotextile filaments allowed for an interbedding hook and loop interaction to take place between both the micro- and macro-scale textures. Initial wear of the geomembrane micro-texture features was responsible for the significant post-peak softening of the coextruded specimens as compared to the

higher strength, stiff structured specimens at low stress levels (Hebeler et al. 2005). To further investigate interface shear strength development mechanisms, Kim and Frost (2011) tested smooth (GMS) and textured geomembranes against geotextiles. For GMS-GT interfaces, predominantly sliding and ploughing components of friction were observed for normal stress ranges of 10-100 kPa and 200-400 kPa, respectively. For GMT-GT interfaces, the response was dependent on gripping configurations of the GTs (constrained and unconstrained) in the tests. Peak and post-peak strengths were lower for the unconstrained than constrained GT due to dilation of the GT filaments along the unconstrained interface and stiffening of the GT filaments along the constrained interface.

Limited quantitative data are available on relative surface texture characteristics of geosynthetics pre- and post-shear. Frost and Lee (2001) provided variations in surface roughness parameter R_s, (quotient of the actual area of a surface to projected area of a surface) for smooth and textured geomembranes tested against geotextiles. The R_s values were determined from 2D profiles of the geomembranes measured using optical microscopy (Gokhale and Underwood 1990, Gokhale and Drury 1990). The R_s decreased due to shearing by 0.4 to 2.1%, 0.8 to 17.9%, and 1.0 to 6.0% for slightly, moderately, and heavily textured geomembranes, respectively, whereas the R_s remained relatively unchanged for the GMS tested against the geotextile (Frost and Lee 2001). Hanson et al. (2015) reported that surface texture of GMTs (determined using optical interferometry) changed significantly against nonwoven GCLs due to shearing where average surface roughness (S_a) of GMTs reduced by 41 and 29% at 20 and 40°C, respectively compared to virgin surface roughness. Peak, core, and valley characteristics of the surface textures and spacing of the texture features also varied due to shearing. Peak material of the textures (S_m) decreased by between 31 and 35%; the heights of the core surface material (S_k) were attenuated by 46 to 53%; and valley material of the textures (S_v) decreased by 52 and 56% (Hanson et al. 2015).

Optical interferometry, a non-contact surface texture analysis method, was used to investigate variations in surface characteristics of geomembranes prior and subsequent to interface shear testing in this study. Pre- and post-shear surface characteristics were analyzed in detail. Comparisons were made between the measured surface texture parameters and shear parameters. The quantified change in surface roughness for each specimen was ultimately used to describe the shear strength response of the tested specimens within a surface texture framework.

2. TESTING PROGRAM

The testing program consisted of determination of surface texture characteristics of pre- and post-shear geomembrane specimens using optical interferometry. The response of two interfaces, geonet (GN)-smooth geomembrane (GMS) and geocomposite (GC)-textured geomembrane (GMT), were determined using a unified inclined plane procedure.

2.1 Materials

The properties of the four geosynthetics used in the test program are presented in Table 1. The materials represented typical products commercially available in Europe. The GC used in the test program consisted of an outer GT encasing a GN drainage core. The geotextile component of the GC was a needle punched, nonwoven product with thickness at 2 kPa of 1 mm and mass per unit area of 130 g/m^2. The geonet component of the GC had identical properties to the GN presented in Table 1.

Table 1. Properties of geosynthetics used in the test program.

Geosynthetic	Material Details	Manufacturer	Thickness at 2 kPa (mm)	Mass per Unit Area (g/m^2)
Geomembrane (GMS)	Smooth (HDPE)	Maccaferri Inc.	2.0	2000
Geomembrane (GMT)	Textured (HDPE)	Maccaferri Inc.	2.0	-
Geonet (GN)	Thermobonded rhomboidal shape (HDPE)	Maccaferri Inc.	3.5	520
Geocomposite (GC)	GT (external filter) + GN (drainage core)	Maccaferri Inc.	6.2	600

2.2 Inclined Plane Tests

The shear behavior of the two interfaces was determined using an inclined plane interface shear testing apparatus. The inclined plane test is generally used to define interface shear strength properties of specimens at low normal stress

levels (<10 kPa) (Lalarakotoson et al. 1999, Wasti and Özdüzgün 2001, Pitanga et al. 2011). The tests were conducted at the LTHE laboratory (University of Grenoble) using an inclined plane apparatus with an upper box supporting an attached geosynthetic sliding along an inclined ramp supporting a second geosynthetic that was properly fixed to the lower plane by means of a clamp system (Figure 1). The dimensions of the apparatus were: L_u = 0.18 m and B_u = 0.70 m for the upper box and L_l = 1.30 m and B_l =0.80 m for the lower support, where L and B represent length (parallel to shearing direction) and width (perpendicular to shearing direction) of the components, respectively (Gourc and Reyes Ramirez 2004). The configuration of the apparatus was similar to standard experimental conditions (EN ISO 12957-2) in that the vertical stress, $\sigma_{v0,}$ remained constant throughout the test and the plane was progressively inclined at a constant rate ($d\beta/dt$ = 3.0 ± 0.5°/min). Vertical stress of 5 kPa was applied by means of metal plates inside the upper box; consequently, the normal stress, $\sigma_v = \sigma_{v0} \cdot \cos\beta$, decreased as the plane inclination (β) increased. The applied vertical stress of 5 kPa was deemed representative of landfill cover conditions using a compacted soil density of 17 kN/m^3 and cover thickness ranging from 0.30 to 0.70 m (vertical stress ranging between 5 and 12 kPa) (Carbone 2014). The following measurements were made during a given test: time, plane inclination angle, upper box acceleration, upper box displacement, as well as the force required to restrain the upper box. Further details related to the apparatus are presented in Carbone et al. (2013a).

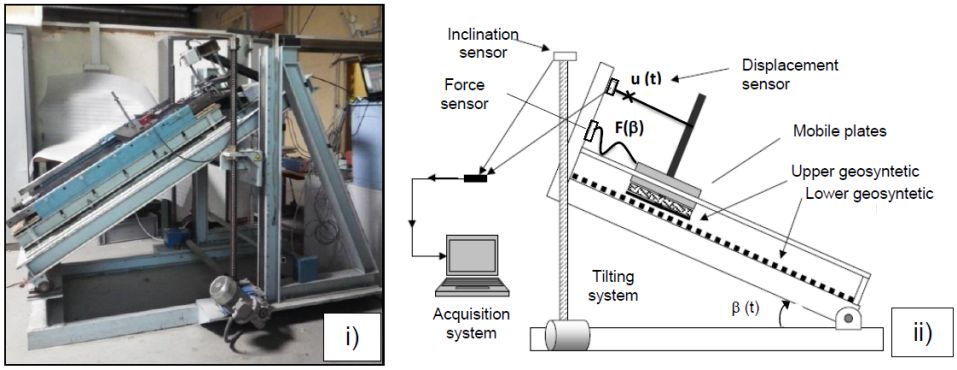

a) Photograph b) Schematic

Figure 1. Inclined plane test apparatus (LTHE, Grenoble University).

The Unified Inclined Plane Procedure (UIPP) was used in this study (Carbone 2014) to overcome limitations of previous procedures presented in Gourc and Reyes Ramirez (2004) and Briançon et al. (2011). The UIPP test followed a three-step procedure to determine three shear strength parameters: the static interface friction angle (δ_o), the dynamic interface friction angle (δ_{dyn}), and the limit interface friction angle (δ_{lim}). Following this procedure, during step 1 (the static phase), δ_o was determined at the inclination angle (β_o) when the upper box first started sliding along the lower geosynthetic support. In step 2, the upper box began accelerating to a constant velocity and δ_{dyn} was determined according to the type of motion induced. According to Gourc and Reyes Ramirez (2004), the interface shear strength mobilization during the slide occurs through three defined mechanisms: sudden sliding, jerky sliding, and gradual sliding. When the limiting displacement was reached ($u = u_{lim}$), the force sensor cable became taut and the box came to rest in a stationary position. Step 3 involved a continuous measurement of force as the plane continued to tilt at a very slow speed ($d\beta/dt$ = 3.0°/min), allowing inertial forces to be considered negligible (Briançon et al. 2011). The force increased with the inclination until stabilization was reached and a constant value of the friction angle (δ_{lim}) was determined (Carbone et al. 2013b).

Wear resistance was characterized by repeating inclined plane tests (i.e., conducting additional shear passes with the same specimens) at the same stress conditions (i.e., 5 kPa). Throughout testing, the geomembrane specimens were affixed to the lower support and the GC or the GN was attached to the upper support. For the GMS-GN interface, six successive shear passes were completed, while the GMT-GC interface was subjected to only three repeated shear passes. The number of shear passes was reduced for the GMT-GC interfaces since surface damage was expected to occur at lower shear displacement levels for the textured geomembrane. For both interfaces tested, in the present paper, only static friction angles were considered. The changes in the shear strength properties were evaluated using a cumulative damage index (DI_{cum}) defined as the percent difference in the tangents of the interface friction angles from virgin to tested conditions (Eq. 1). Also, an incremental damage index (DI_{inc}) was introduced as the percent difference in the tangents of the interface friction angles from selected successive shear passes (Eq. 2). These indices were applied to δ_o, as the static interface friction was determined to be highly sensitive to wear (Carbone 2014). Positive values of DI indicated loss of interface friction with progressive shear passes, whereas negative values indicated interface friction gain with progressive shear passes.

$$DI_{cum} = \frac{(\tan\delta_{virgin} - \tan\delta_{tested})}{(\tan\delta_{virgin})} * 100 \quad [1]$$

$$DI_{inc} = \frac{(\tan\delta_{m} - \tan\delta_{n})}{(\tan\delta_{m})} * 100 \quad [2]$$

where m = earlier shear pass number and n = later shear pass number. For GMS-GN interface, the interface friction angles and DI values were determined for the virgin (i.e., 1st), 4th, and 6th passes and for the GMT-GN interface, values were determined for virgin (i.e., 1st), 2nd, and 3rd passes.

2.3 Surface Texture Tests

Optical interferometry is a non-contact method for surface texture quantification. The scale of height and lateral measurement ranges from nano to macro scale on a given surface (Bruker-Nano 2011). This range in height and lateral resolution is obtained from analysis of interference patterns produced from a coherent light source (i.e., white or green broadband light) and an interferometric lens (at a specified magnification). Surface texture quantification relies on both 2D and 3D analysis at four different scales of measurement: primary (i.e., raw data with measurement noise attenuated), roughness, waviness, and form (Whitehouse 2011). Short pass, long pass, and band pass Gaussian filtering are used to extract the various scales. Two-dimensional surface texture analysis includes texture quantification along a linear profile (in either a specified x or y direction), while three-dimensional analysis incorporates quantification along a given plane in both the x and y directions. Each scale of measurement may be important for different contact applications, and analyzing a variety of surface texture parameters at each scale is warranted. The interferometer used in this test program was a Bruker NP-Flex and the surface texture analysis software was Vision 64. Different measurement settings were used for smooth and textured materials. The vertical scan length for the GMS was set at 500 μm as compared to a longer vertical scan length of 1200 μm for the GMT surfaces. Similarly, the backscan length was set at 5 μm for the GMS surfaces and 15 μm for the GMT surfaces. The modulation threshold was set to 2%. The illumination source was set to the green narrow band setting at 100% intensity, as the analyzed surfaces were black and non-reflective.

For the test program, a total of 5 random areas on the surface of each geomembrane specimen were analyzed. Each test area had dimensions of 50 mm by 2 mm. One of the random areas was chosen in close proximity to the middle of each specimen (close to the primary/initial shear zone) to properly assess the spatial variability of surface texture deformations on the geomembrane surface. The 50 mm length was ascertained based on geomembrane surface analysis testing recommendations provided by Yesiller and Cekic (2005) obtained using optical microscopy. The testing length also was confirmed by preliminary testing on a textured geomembrane using the interferometer. The 50 mm length was aligned parallel to the machine direction (i.e., sliding direction) on the test specimens. The field of view for each individual image was set at 1.1 mm x 0.80 mm. Automatic stitching of images was used to obtain the full measurement areas. In total, 142 individual stitched images were required for each 50 mm by 2 mm test area. Two measurement scales were investigated in detail for both the virgin and tested geomembrane specimens including the primary and roughness scales of analysis. The primary and roughness scales were obtained using long pass and band pass Gaussian regression filtering, respectively. Lower cutoff values (λ_s = 0.06 to λ_c = 0.6 μm) were used for GMT than GMS (λ_s = 0.3 to λ_c = 3 μm) since the rougher texture resulted in a larger number of higher frequency, low amplitude texture features and measurement noise. The defined bandwidth (λ_s to λ_c) of each bandpass filter used was kept at a constant 1:10 ratio, which is a typical filter setting for most surface texture applications (Whitehouse 2011).

Both 2D (i.e., along lines-linear, R parameters) and 3D (i.e., about planes-areal, S parameters) texture parameters were used in this investigation. The amplitude parameters are used for quantifying height distribution of a surface about a mean line or reference plane. The spatial parameters are used for quantifying the spacing between given features on a surface. The hybrid parameters integrate both spacing and amplitude (e.g., slope) to characterize surface features. Lastly, the functional parameters are used for predicting or quantifying a given function/performance of a surface (i.e., fluid retention properties or contact mechanics) and are based on material ratio curves (Whitehouse 2011).

The two most widely used amplitude parameters in 3D analysis are S_a and S_q. S_a is the average roughness evaluated over a given 3D surface, or the average absolute value of the surface deviations about a mean plane. S_q is the root mean square (RMS) of the average deviations evaluated over a given 3D surface about a horizontal best-fit plane. S_{sk} and S_{ku} represent the statistical skewness and kurtosis, respectively of the surface texture of the measured 3D surface. S_{sk} indicates the relative degree of symmetry of all measured surface heights about a mean plane (x, y direction), while S_{ku} measures the presence of outliers (extremely high/deep peaks/valleys) throughout the surface (Cohen 2004). The 2D and 3D spatial texture parameters are associated with quantifying the spacing between prominent surface texture features or the horizontal characteristics of the surface deviations. In 2D analysis, RS_m is the mean spacing between profile peaks at the mean line calculated between regions where a local valley and peak exist and PW is the peak width measured at the mean line of the surface profile. The 3D spatial parameters investigated included S_{td} or the texture direction of the surface. S_{td} is derived from the angular power spectral density function (APSDF) and is a measure of the angular direction of the dominant lay comprising a surface (Cohen 2004). The S_{td} parameter is evaluated along an

imaginary y-axis placed parallel to the sliding plane. A surface with a lay along the y-axis corresponds to S_{td} = 0, while a surface that is directional may have a negative or positive value. Surfaces that are spatially random and highly variable have an indeterminate S_{td} value (Cohen 2004). The hybrid 3D parameters incorporate spatial and amplitude characteristics of a given surface texture. S_{dq} is the root-mean square surface slope, and is a measurement of all slopes which comprise the 3D surface in both the x and y directions. S_{dr} is defined as the developed surface area ratio, and represents the area created from the surface texture itself as compared to a flat plane. In general, S_{dr} values will increase with spatial intricacy of the texture. The measured absolute surface area (SA) is the total exposed 3D surface area, including the surface area of peak and valley features (Cohen 2004).

Functional parameters were developed in relation to the use of a given material (Whitehouse 2011). These parameters are critical in the design of surface texture for contact applications to predict performance of the surface (wear, adhesion, etc.) over time. All of the functional parameters are dependent on the areal material ratio curve. The areal material ratio curve (also known as the bearing area curve) is generated by assuming that a horizontal plane is progressively moving from the highest peak (0% contact area) to the lowest valley (100% contact area) on the surface. The percentage of contact area that the horizontal plane makes with the surface is quantified throughout the full height of the surface (Figure 2). The shape of the curve provides indication of functional performance described by parameters S_m, S_{cm}, and S_v (Cohen 2004). S_m represents the peak material volume and is defined as the volume of material contained in the surface peaks at 10% contact area on the bearing ratio curve. S_{cm} is defined as the core material volume, or the surface texture material existing between 10 and 80% of the areal material ratio curve. Comparably, the valley void volume (S_v) is the volume of voids between 80 and 100% of the bearing ratio or the amount of fluid that fills the valleys on the surface beyond the 80% contact area limit. In addition, the natural volume (NV) is determined as the volume occupied between the surface and a reference plane placed at the elevation of the highest peak parallel to plane of the measured surface (Bruker-Nano 2011). The NV represents the volume of fluid the surface supports for complete submersion.

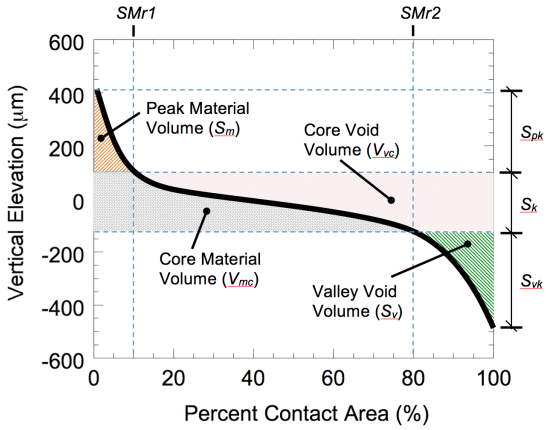

Figure 2. Areal material ratio curve.

3. RESULTS AND DISCUSSION

3.1 Inclined Plane Tests

The inclined plane test on GMS-GN interface resulted in an increase in the interface friction angles with an increasing number of shear passes (Table 2). The static interface friction angle was observed to increase, resulting in negative DI values as low as -22.1%. Modifications to the surfaces of the smooth geomembranes were visually observed. The trends of upper box displacement versus plane inclination angle for each of the shear passes, as presented graphically by Carbone (2014), indicated that progressive wear was occurring due to shearing. The sliding displacements were relatively gradual for the first shear pass, whereas a combination of jerky-sudden sliding was observed for the 6th pass. The mobilized friction was relatively constant for the 6th pass as compared to the 1st pass. Therefore, even though shear testing resulted in an increase in relative strength properties with increasing shear passes, a progressive wear pattern was observed for the GMS-GN interface. By the end of the 4th shear pass, the previous indentations and peak formations appeared to have resulted in gripping the GN interface at a given angle yet an almost instantaneous failure occurred when the inclination was increased even slightly. The progressive roughening of the GMS surface as a result of the abrasive wear of the hard GN ribs on the smooth GMS surface increased the shear resistance of the GMS-GN interface. Areas of extreme texture change (e.g., pit and peak formation) may have been a result of jerky sliding at the interface,

where the GN ribs may have stopped suddenly thereby indenting material to a greater extent than that of the spatially oriented indentations resulting from prior shear passes.

Inclined plane tests on the GMT-GC interface resulted in a decrease in the static interface friction angle (δ_o) with an increasing number of shear passes resulting in DI_{cum} values up to +24.8% (Table 2). Modifications to the surfaces of the textured geomembranes and geocomposites were visually observed. The trends of upper box displacement versus plane inclination angle for each of the shear passes, as presented graphically by Carbone (2014), indicated that progressive wear was occurring on the interfaces. The displacement was generally gradual followed by an accelerated motion. As the number of shear passes increased, a larger range of gradual upper box displacement was encountered before sudden sliding occurred. The interface behavior was attributed to a change in surface texture of the GMT combined with a breakage of filaments of the GC. The effectiveness of hook and loop interaction between the geosynthetics was reduced with increasing shearing displacements. Similar to GMS-GN interface, an asymptotic trend towards a final worn surface was observed with decreasing DI_{inc} with increasing number of shear passes.

Table 2. Inclined plane shear test data.

Interface tested	Number of Shear Passes	δ_o (°)	Static DI_{inc} (%)	Static DI_{cum} (%)
GMS-GN	Virgin	13.3	N/A	N/A
	4th	14.2	-7	-7
	6th	16.1	-13	-22
GMT-GC	Virgin	38.2	N/A	N/A
	2nd	32.8	+18	+18
	3rd	30.6	+8	+25

3.2 Surface Texture Tests

Surface texture parameters were evaluated for the GMS surface for pre- and post-shear conditions at both the primary and roughness scales. The roughness scale provided representative assessment of changes in microtexture features of the GMS surface (Table 3). Example images of pre- and post-shear GMS surfaces are presented in Figure 3. The amplitude parameters S_a and S_q increased significantly subsequent to the interface tests indicating roughening of the GMS surface (Table 3). The surface roughening was mainly attributed to valley formation: i) spatially oriented indentations of constant depth and width generally parallel to the sliding direction and ii) random areas of deep pitting. Decreasing skewness (S_{sk}), increasing void volume of valleys (S_v), increasing natural volume (NV), and the development of a preferential texture direction parallel to the direction of shearing (S_{td}) for the tested specimens also indicated formation of valley features on the GMS (Table 3, Figure 3).

Table 3. Summary of 2D and 3D surface texture parameters for the GMS specimens at the roughness scale.

Parameter	Unit	Virgin		Tested		
		μ	COV (%)	μ	COV (%)	Δ%
S_a	μm	0.739	7	1.24	39	68
S_q	μm	1.03	7	3.04	75	193
S_{sk}	-	-0.70	193	-0.34	904	-52
S_{ku}	-	13	109	52.7	78	305
RS_m	μm	1877	17	5294	80	182
S_{td}	°	-17.9	78	-1.2	63	93
S_{dq}	°	0.69	10	1.46	42	112
SA	μm^2	9.99E+07	0	1.00E+08	0.03	0.1
S_m	μm	0.06	29	0.21	112	275
S_{cm}	μm	1.17	9	1.63	32	40
S_v	μm	0.13	10	0.36	67	179
NV	μm^3	2.18E+08	11	3.74E+08	93	72

In addition, formation of extreme peaks was observed, usually i) at the end of a spatially oriented indentation, ii) on the sides of an indentation, or iii) surrounding a pit formation. The formation of peaks on the tested GMS surfaces was supported by an increase in kurtosis (S_{ku}) values, indicating increased presence of high peaks and increases in positive volume and peak/core material volumes (S_m/S_{cm} values) (Figure 4a). Increased slope (S_{dq}) of texture features indicated sharp and irregular peaks, rather than smooth and rounded peaks. Consolidation of multiple peaks into larger composite

surface features also was observed, with an increase in prominent peak and valley spacing (RS_m). In addition, ironing of the individual asperities on the geomembrane surface was observed supported by an increase in prominent peak spacing (RS_m). This ironing effect may have resulted from elastoplastic deformation of peak features. The deformation causing merging of individual features was induced by the interaction of the ribs of the geonet and the GMS when the angle of contact between the two geosynthetics was relatively low (i.e., two surfaces were relatively parallel) (Briscoe et al. 1996). Ironing effects also may have resulted from prolonged sliding contact, rather than ploughing at the interface (Briscoe 1998). At the primary scale, prominent peak formations (at the prow of ploughing tracks) generally ranged from 44 to 110 µm in height, peak formations to the side of ploughing tracks and pits ranged from 9 to 25 µm in height, indentations ranged from -19 to -48 µm in depth, while pit formations ranged from -77 to -109 µm in depth. At the roughness scale, prominent peak formations (at the prow of ploughing tracks) generally ranged from 65 to 103 µm in height, peak formations to the side of ploughing tracks and pits ranged from 4 to 12 µm in height, indentations ranged from -10 to -11 µm in depth, while pit formations ranged from -40 to -65 µm in depth.

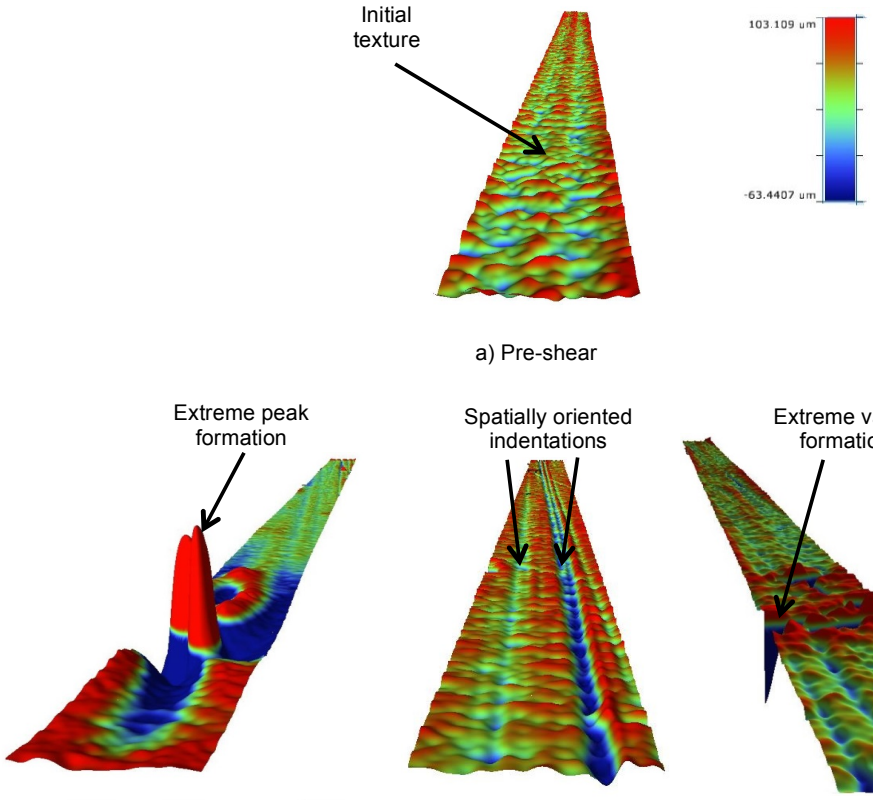

Figure 3. Examples of GMS surfaces (2 mm x 50 mm areas).

Significant variations to the surface of the GMS were observed due to shearing, yet the absolute surface area (SA) remained relatively similar between pre- and post-shear specimens (Table 3). Elastoplastic surface deformations are considered to conserve material volume at an interface yet result in rearrangement of the surface features with permanent indentations (Briscoe et al. 1996). The roughening of the GMS surfaces likely resulted from similar processes. Briscoe et al. (1996), Briscoe (1998), and Myshkin et al. (2005) described combined indenting wear as viscoelastic-plastic ductile ploughing, where the indentor causes a certain depth of plastic deformation (producing a groove), and viscoelastic recovery occurs with material pushed to the sides of the groove, and a prow is generated at the head of the groove. The stiff ribs of the GN formed permanent random areas of scratching without removing polymer material from the GMS surface. Polymer material likely was pressed deep into the GMS surface by the GN ribs, displacing the GMS polymer into irregular, random peaks. The relatively rounded/smooth GN ribs, the lack of contrast between hardness of the interfacing surfaces, and the low confining stress conditions used for testing likely resulted in permanent deformation of the GMS surface without any tears, cutting, or removal of material.

The surface texture characteristics of the GMT for pre- and post-shear conditions were analyzed at the primary and roughness scales of measurement (Table 4). The trends in the variations of the surface characteristics at the two measurement scales were similar and results from the roughness scale are presented in detail herein. Example images of pre- and post-shear GMT surfaces are presented in Figure 5. The amplitude parameters S_a and S_q increased subsequent to the interface tests indicating roughening of the GMT surface (Table 4). Similar to the observations for GMS, valley feature formation was more prominent than peak formation on the GMT. This observation was supported by a decrease in skewness (S_{sk}) suggesting the data was skewed more towards valley features than peak features upon shearing and also supported by an increase in valley void volume on the surface (S_v). Post-shear decrease in kurtosis (S_{ku}) indicated reduced extreme peak and valley features (Table 4). The spacing of prominent peak features (RS_m) also decreased as well as a decrease in peak width (PW). Both interfacial area (S_{dr}) and absolute surface area (SA) increased for the tested GMT surface. The peak material volume (S_m) decreased and the core material volume (S_{cm}) increased indicating removal of peak material and possible deposition of the deformed/removed peak material on the core surface (Figure 4b). Finally, the increase in natural volume (NV) likely resulted from the fraying of the microtexture on the GMT macrotexture features. Extra void volume was created as peak material was broken off into more jagged features. At the roughness scale, the maximum height of the peaks increased from 309 μm to 405 μm and the core material volume increased from 41 μm to 74 μm, whereas at the primary scale the maximum height of the peaks increased from 623 to 783 and the core volume increased from 133 μm to 225 μm.

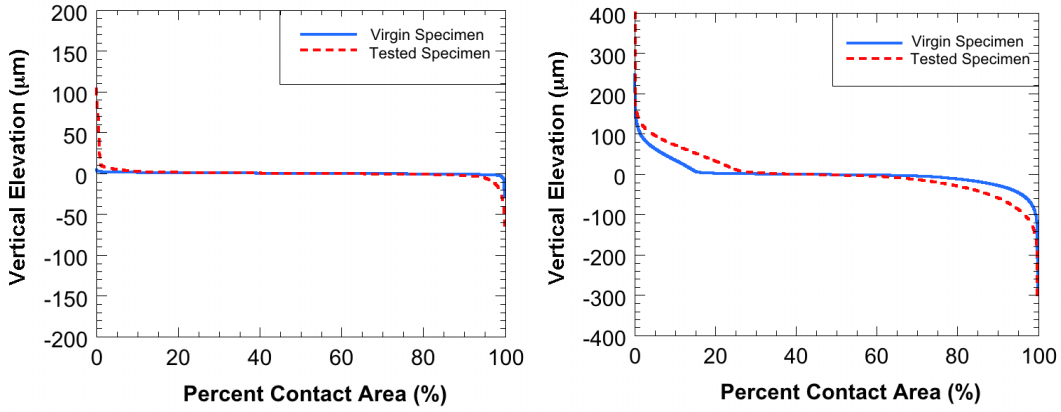

a) GMS b) GMT

Figure 4. Areal material ratio curves for GM specimens.

Table 4. Summary of 2D and 3D surface texture parameters for the GMT specimens at the roughness scale.

Parameter	Unit	Virgin		Tested		
		μ	COV (%)	μ	COV (%)	Δ%
S_a	μm	29.2	30	35.7	11	78
S_q	μm	46.5	24	55.3	10	55
S_{sk}	-	0.532	52	0.33	50	-66
S_{ku}	-	6.23	35	5.34	14	-40
RS_m	μm	2102	20	1581	7	-25
PW	mm	0.617	22	0.472	24	-23
S_{dq}	°	43.4	20	59	6	37
S_{dr}	-	42.2	56	112	24	166
SA	μm^2	1.24E+08	9	1.53E+08	6	23
S_m	μm	3.55	15	3.53	14	-1
S_{cm}	μm	40.9	45	74	10	80
S_v	μm	5.01	24	7.52	8	50
NV	μm^3	1.10E+10	16	1.44E+10	9	31

For the GMS-GN interface, abrasive wear of the hard GN ribs on the smooth GMS surface resulted in increased roughness of the GMS surface. The static interface friction angle corresponding to onset of sliding increased with increasing shear passes from 13.3 to 16.1° (Table 2) due to the increased roughness. However, excessive roughening and wear at large displacements may result in potential for strain-softening behavior. Angled indentations (with respect to sliding direction) observed from interferometry data indicated potential lateral sliding during shearing. For the GMT-GC

interface, the static interface friction angle at the onset of sliding decreased with increasing shear passes from 38.2 to 30.6°. The interactions at this interface were more complex than the interactions for the GMS-GN. Progressive shear passes caused roughening of the GMT surface. Even though the roughness of the GMT increased subsequent to shear as indicated by the measured average and RMS surface roughness values (Table 4), the shear resistance of the interface decreased with increased displacement. The overall deformation mechanism of the GMT surface was attributed to the abrasive wear between the geotextile filaments of the GC and the microtexture existing on the macro asperity features. Relatively low variations were observed in the macro asperity structures (i.e., primary scale), whereas higher variation was observed for the microtexture (i.e., roughness scale), which controlled the interface behavior. The filaments of the nonwoven geotextile in the GC entangled with and deformed the asperities on the geomembrane surface with a hook and loop mechanism. Geotextile filaments were visible on the GMT surface after shearing. In addition, the interlocking of filaments with the microtexture features on the asperities caused damage to the GMT surfaces and an overall "fraying" effect. The increase in relative peak heights and decrease in peak widths provided quantitative extent of the fraying effect. With increasing number of shear passes, the level of surficial interaction likely decreased and the filaments continued to deform the microtexture on the macro asperity features resulting in elongated, jagged peaks (Figure 5). As sliding occurred over multiple shear passes, the filaments likely penetrated the surface to a deeper extent, roughening the core texture and increasing void volume of valley features immediately surrounding the macro asperities. The smaller changes in DI_{inc} with increasing shear passes indicated that the roughening mechanism was asymptotic (i.e., reduced influence with further shear passes). This led to a reduced strain softening effect at higher displacements (i.e., at higher shear pass numbers) as effectively a final worn surface texture was approached.

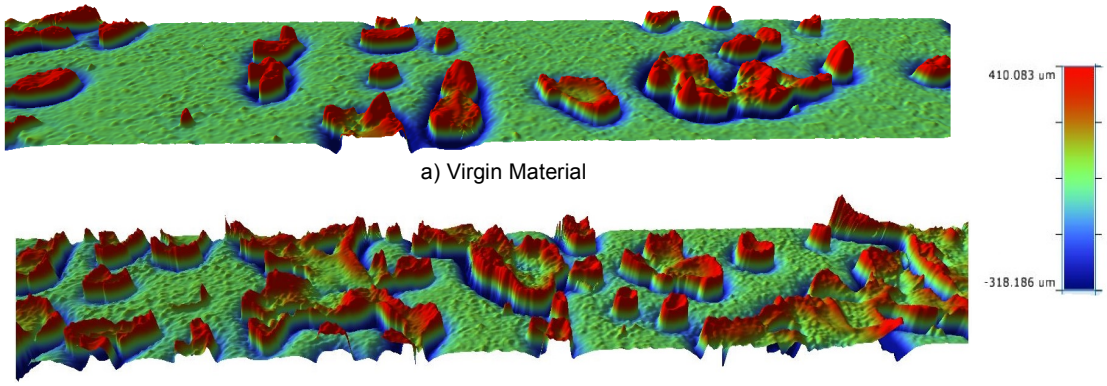

a) Virgin Material

b) Tested Material

Figure 5. Examples of GMT surfaces (zoomed in 2 mm x 8 mm areas).

4. CONCLUSIONS

Optical interferometry, a non-contact analysis method, was used to investigate variations in surface characteristics of geomembranes subsequent to interface shear tests. The shear strength of two interfaces, smooth geomembrane (GMS)-geonet (GN) and textured geomembrane (GMT)-geocomposite (GC), were determined using an inclined plane test procedure with repeated shear passes at 5-kPa vertical stress representing landfill cover conditions on slopes. 2D and 3D surface texture characteristics of the geomembranes were analyzed on virgin and post-shear specimens. Geomembrane surfaces were modified significantly due to the shearing process. For the GMS-GN interface, the static interface friction angle corresponding to onset of sliding increased with increasing shear passes from 13.3 to 16.1°. The overall roughness of the GMS increased during the tests. The GN ribs ploughed into the geomembrane surface resulting in permanent, spatially oriented indentations. Peak and valley features were developed on the GMS surface with pronounced peaks at the end of the indentations along the shear direction. The average and RMS roughness, developed surface area, peak material volume, valley void volume, and natural volume increased, whereas absolute surface area remained similar. GMS surface was permanently textured yet the polymer surface material was conserved. For the GMT-GC interface, the static interface friction angle at the onset of sliding decreased with increasing shear passes from 38.2 to 30.6°. The filaments of the nonwoven geotextile in the GC entangled with and deformed the asperities on the geomembrane surface. The width of the peak features decreased and the height of the peaks, depth of the valleys around the peaks, negative volume, and absolute surface area increased. The elongated peak features resulted in decreased contact potential with the overlying GC. The overall increase in the roughness of the GMS resulted in the increased shear strength, whereas the specific mechanism of deformation of the GMT surface features caused the decreased shear strength. Overall, consistent trends were observed between friction behavior based on the inclined plane test and surface texture response based on optical interferometry.

5. ACKNOWLEDGEMENTS

The study was partially supported by an MRI award from the National Science Foundation (CMMI-1039995) and the Global Waste Research Institute. The authors also acknowledge Officine Maccaferri Inc. for supplying test materials.

6. REFERENCES

Briançon, L., Girard, H., and Gourc, J.P. (2011). A new procedure for measuring geosynthetic friction with an inclined plane, *Geotextiles and Geomembranes*, 29: 472–482.

Briscoe, B.J., Evans, P.D., Pelillo, E., and Sinha, S.K. (1996). Scratching maps for polymers, *Wear*, 200: 137-147.

Briscoe, B.J. (1998). Isolated contact stress deformation of polymers: the basis for interpreting polymer tribology, *Tribology International*, 31(1-3): 121-126.

Bruker-Nano Inc. (2011). *Guide to Surface Texture Parameters as Used in the Vision 64 Program*.

Carbone, L. (2014). Interface behaviour of geosynthetics in landfill cover systems under static and seismic loading conditions, Ph.D. Dissertation, Mediterranea University of Reggio Calabria, Italy and University of Grenoble, France.

Carbone, L., Gourc, J.P., Carrubba, P., Moraci, N., Briançon, L., Pavanello, P. (2013a). New perspectives in the interface shear strength characterization through the inclined plane test, *Proceedings Sardinia 2013, Fourteenth International Waste Management and Landfill Symposium*, S. Margherita Di Pula, Cagliari, Italy.

Carbone, L., Gourc, J.P., Briancon, L., Moraci, N., and Carrubba, P. (2013b). What value of interface friction to select for geosynthetic liner on landfill slopes? *Proceedings of Geosynthetics 2013,* Long Beach, California, USA.

Cohen, D.K. (2004). *Glossary of Surface Texture Parameters,* Application Notes, Michigan Metrology Inc., LLC.

Frost, J.D. and Lee, S.W. (2001). Microscale study of geomembrane-geotextile interactions, *Geosynthetics International*, 8(6): 577-596.

Gokhale, A.M. and Drury, W.J. (1990). A general method for estimation of fracture surface roughness: Part II practical considerations, *Metallurgical Transactions A,* 21A: 1201-1207.

Gokhale, A.M. and Underwood, E.E. (1990). A general method for estimation of fracture surface roughness: Part I theoretical aspects, *Metallurgical Transactions A,* 21A: 1193-1199.

Gourc, J.P., and Reyes Ramìrez, R. (2004). Dynamics-based interpretation of the interface friction test at the inclined plane, *Geosynthetics International*, 11: 439–454.

Hanson, J.L., Chrysovergis, T.S., Yesiller, N., and Manheim, D.C. (2015). Temperature and moisture effects on GCL and textured geomembrane interface shear strength, *Geosynthetics International*, accepted for publication.

Hebeler, G.L., Frost, J.D., and Myers, A.T. (2005). Quantifying hook and loop interaction in textured geomembrane-geotextile systems, *Geotextiles and Geomembranes*, 23: 77-105.

Jones, R. and Dixon, N. (1998). Shear strength properties of geomembrane/geotextile interfaces, *Geotextiles and Geomembranes*. 16: 45-71.

Kim, D. and Frost, J.D. (2011). Effect of geotextile constraint on geotextile/geomembrane interface shear behavior, *Geosynthetics International*, 18(3): 104-123.

Koerner, R.M. (2005). *Designing with Geosynthetics*, Prentice Hall, Upper Saddle River, NJ.

Lalarakotoson, S., Villard, P., Gourc, J.P. (1999). Shear strength characterization of geosynthetic interfaces on inclined planes, *Geotechnical Testing Journal,* 22: 284 - 291.

Li, M.H. and Gilbert, R.B. (2006). Technical Note: Mechanism of post-peak strength reduction for textured geomembrane-nonwoven geotextile interfaces, *Geosynthetics International*, 13(5): 206-209.

Moraci, N., Cardile, G., Gioffré, D., Mandaglio, M.C., Calvarano, L.S., Carbone, L. (2014). Soil geosynthetic interaction: design parameters from experimental and theoretical analysis, *Transportation Infrastructure Geotechnology*, 1(2): 165-227.

Myshkin, N.K., Petrokovets, M.I., and Kovalev, A.V. (2005). Tribology of polymers: Adhesion, friction, wear, and mass-transfer, *Tribology International*, 38: 910-921.

National Research Council – NRC. (2007). *Assessment of the Performance of Engineered Waste Containment Barriers*, The National Academies Press, Washington D.C.

Palmeira, E.M. (2009). Soil–geosynthetic interaction: Modeling and analysis. *Geotextiles and Geomembs.,* 27: 368-390.

Pitanga, H.N., Gourc, J.P., and Vilar, O.M. (2011). Enhanced measurement of geosynthetic interface shear strength using a modified inclined plane device, *Geotechnical Testing Journal*, ASTM, 34(6): 643-652.

Qian, X., Koerner, R.M. and Gray, D.H. (2002). *Geotechnical Aspects of Landfill Design and Construction*, Prentice Hall, Upper Saddle River, NJ.

Triplett, E.J. and Fox, P.J. (2001). Shear strength of HDPE geomembranes/geosynthetic clay liner interfaces, *Journal of Geotechnical and Geoenvironmental Engineering*, ASCE, 127(6): 543-552.

Wasti, Y. and Özdüzgün, Z.B. (2001). Geomembrane - geotextile interface shear properties as determined by inclined board and direct shear box tests, *Geotextiles and Geomembranes*, 19: 45-57.

Whitehouse, D.J. (2011). *Handbook of Surface and Nanometrology*, 2nd ed., Taylor & Francis, New York.

Yesiller, N. and Cekic, A. (2005). Determination of surface and thickness characteristics of textured geomembranes using image analysis, *Geotechnical Testing Journal*, ASTM, 28(3): 275-287.